Supplemental Information for Basic Features of a Cell Electroporation Model: Illustrative Behavior for Two Very Different Pulses

Basic features of a cell electroporation model: Illustrative behavior for two very different pulses

Reuben S. Son, Kyle C. Smith, Thiruvallur R. Gowrishankar, P. Thomas Vernier and James C. Weaver

Supplemental Information (SI)

Idealized and actual pulse waveforms

To aid understanding we use idealized pulse waveforms. The pulses are trapezoidal, with linear ramps that define the rise and fall times, and a flat peak field strength. Again for simplicity, we label a pulse duration by the duration from start to end. The model can also be used with digitized experimental waveforms. Significant averaging occurs in computing cumulative solute transport, which supports our use of idealized waveforms for understanding basic behavior. There is underlying spatial averaging of $U_{\mathrm{m}}(t)$ behavior that is are distributed over several hundred transmembrane node-pairs, and also integrating the solute transport rates with respect to time. **Fig. SI-1** shows the two idealized pulse waveforms used here.

Field amplification by a cell membrane

Fig. SI-2 shows the model's field amplification for both the passive (fixed membrane properties as in the Schwan model) and active properties (resting potential source and the dynamic EP model). For both cases the cell membrane effectively amplifies an applied field, such that the membrane response field, E_{m}, is larger than the applied field E_{e}. Field amplification diminishes for rapidly changing waveforms that create significant displacement currents, with dielectric properties then more important than conductive properties. Amplification is complicated once spatially distributed EP occurs, as the effective conductivity of the membrane then changes with location as well as with time.

Traditionally field amplification is defined as the ratio of changes, viz. membrane field change divided by applied field change. However, because of the importance of transmembrane field magnitude $U_{\mathrm{m}}(t) = E_{\mathrm{m}} d_{\mathrm{m}}$ in governing pore creation, we use a slightly different definition: the ratio of membrane field, E_{m} to the applied field. In our version the resting potential source makes a small contribution, which allows direct consideration of the strength, and sometimes polarity, of the local transmembrane voltage, U_{m}.

In cases where we show the response at time where the field pulse changes slope, we use the slope just before that time. This means that the affect of rapid changes in the pulse do represent the times at which dielectric properties are important.

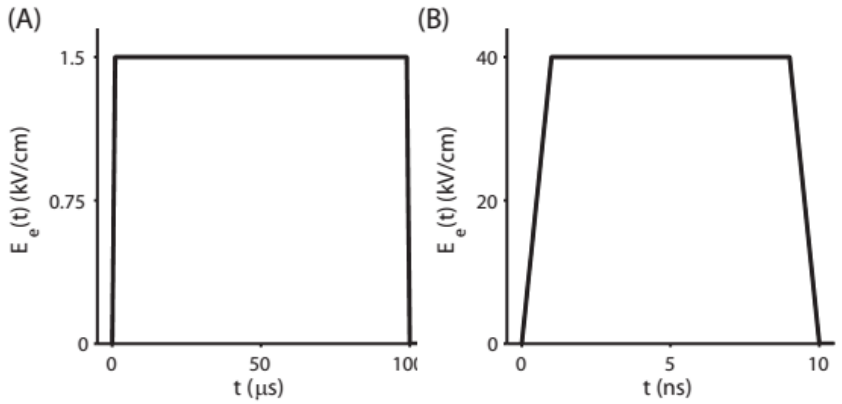

Fig. SI-1 An electric field pulse, $E_e(t)$, is applied via idealized planar electrodes spaced 100 μm apart at the top and bottom of the system model. The results in the following figures are obtained for two different idealized trapezoidal pulses: **(A)** a 1.5 kV/cm, 100 μs rise/fall times; and **(B)** a 40 kV/cm, 10 ns pulse with 1 ns rise/fall times.

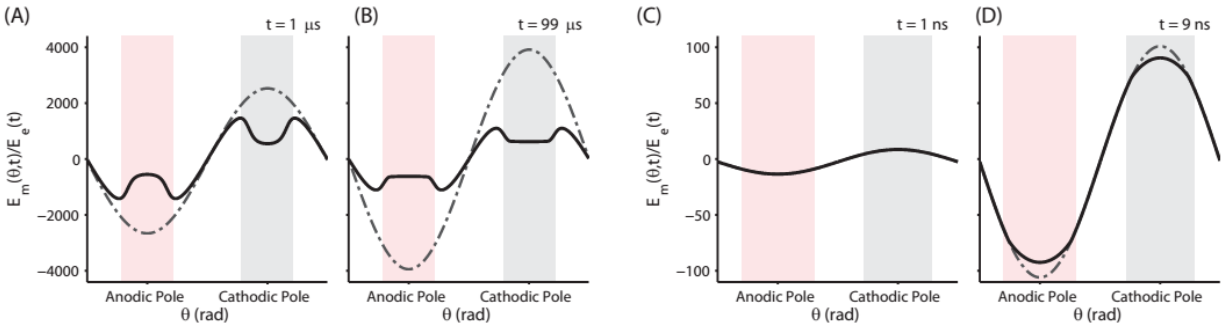

Fig. SI-2 Amplification gain factor, E_m/Ee, is shown as a function of angle at different times. **(A-B)** show the response to a 1.5 kV/cm, 100 μs pulse at the start and end of the pulse maximum. **(C-D)** show the response to a 40 kV/cm, 10 ns pulse at the start and end of the pulse maximum. In all figures, the dash-dotted curve represents the passive membrane amplification response, in which the dynamic electroporation model has been 'knocked out'. In **C**, the two curves are indistinguishable because the onset of electroporation has not yet occurred.

1 Supplemental information regarding June 2015 manuscript revision

In the process of exercising and extending the cell model, we have discovered an error in the software code used to implement the model: one term in the expression for the effective membrane tension, Γ_{eff}, had the wrong sign. The membrane tension is one component in the description of pore energy, and has been employed in essentially all previous electroporation models. The incorrect expression for Γ_{eff} and its correction are discussed in the following pages. To both test our model and revise the manuscript, results have been obtained the comparison of three different expressions for membrane tension: (1) a corrected version of the effective tension, $\Gamma_{\text{eff,cor}}$ (2) a traditional fixed tension, $\Gamma = 10^{-5}$ N/m, and (3) the original incorrect expression for effective tension, $\Gamma_{\text{eff,inc}}$. We also compare results obtained with two different values of the maximum pore radius: $r_{\text{p,max}} = 12$ [1], and a larger value of 60 nm, which is motivated by Krassen et al. [2] and is the value used in the original published manuscript. This led to six simulations (3 versions of Γ and 2 values of $r_{\text{p,max}}$) each for the 1.5 kV/cm, 100 μs and 40 kV/cm, 10 ns pulses studied in the manuscript. Based on these results, we have revised the results and figures in the manuscript with results obtained with the traditional, fixed value of $\Gamma = 10^{-5}$ N/m instead of Γ_{eff} and 12 nm r_{max} instead of 60 nm. These changes yield little quantitative difference in our modeling predictions and do not change the conclusions of the original manuscript.

A detailed discussion of the revision based on comparative results, with accompanying equations, tables and figures, is presented in the following pages. For the majority of cases, we find only minor differences in model predictions of measurable quantities (transmembrane voltage, $\Delta\phi_{\text{m}}$, membrane conductance, G_{m}, and cumulative solute transport, n_{s}). In the comparison of pore size distributions (pore histograms), the usage of maximum pore radius, $r_{\text{max}} = 12$ nm vs. 60 nm yield differences in predicted pore expansion and in presentation. However, these do not significantly affect what is important: predictions of what can be observed in experiments (i.e. solute transport). In addition to comparing model results obtained for the two pulses studied in the original manuscript, we furthermore present comparative model results obtained for conditions used to establish the model [1, 3–5] based on calcein uptake experiments of Canatella et al. 2001 [6] and Lucifer yellow uptake by Puc et al. 2003 [7]. For perspective, the general electroporation literature shows that experimental and theoretical uncertainties are generally greater than 10%, and often much larger.

The mathematical expression for effective membrane surface tension, Γ_{eff} [1, 8] , is

$$\Gamma_{\text{eff}} = 2\Gamma' - \frac{2\Gamma' - \Gamma}{(1 - \frac{A_{l,p}}{A})^2} = 2\Gamma' - \frac{2\Gamma' - \Gamma}{1 - 2\frac{A_{l,p}}{A} + \frac{A_{l,p}^2}{A^2}}. \tag{1}$$

As in recent publications [3–5] $\Gamma' = 20 \times 10^{-3}$ N/m is the interfacial energy per area of the water-hydrocarbon-water interface, Γ is the surface tension of the intact membrane with a fixed value of 10^{-5} N/m [9–11], $A_{l,p}$ is the total reduction in lipid area that results from the creation and evolution of pores, and A is the lipid membrane surface area. Eq. 1 was originally developed [8] to increase membrane surface tension as $A_{l,p}$ increases, motivated by a decrease in membrane area available for EP as the membrane electroporates and pores expand. The interfacial energy of lipid in the membrane, W_{surf}, is then defined as

$$W_{\text{surf}}(r_p) = -\Gamma_{\text{eff}} \delta A_{l,p}(r_p), \tag{2}$$

where $\delta A_{l,p}$ is the reduction in lipid area due to a pore, such that increasing Γ_{eff} shifts the energy landscape to favor greater pore expansion. However, the inadvertent error in implementing Eq. 1 resulted in the following incorrect definition in software:

$$\Gamma_{\text{eff,inc}} = 2\Gamma' - \frac{2\Gamma' - \Gamma}{(\frac{A_{l,p}}{A})^2} = 2\Gamma' - \frac{2\Gamma' - \Gamma}{1 + 2\frac{A_{l,p}}{A} + \frac{A_{l,p}^2}{A^2}}. \tag{3}$$

This error in Eq. 3 changes the sign of the dependence of Γ_{eff} on $A_{l,p}$, which changes the dependence of Γ_{eff} on lipid area in Eq. 2 and results in Γ_{eff} decreasing with increasing $A_{l,p}$. Consequently, the downward shift in the pore energy generated by expanding pores is underestimated, and the prediction for solute influx is diminished.

In Figs. SI-3-14, we present revised results obtained for the two pulses studied in the manuscript (originally published July 22, 2014): a 1.5 kV/cm, 100 μs pulse (characteristic of conventional EP) and a 40 kV/cm, 10 ns pulse (representing nsPEF; nanosecond pulsed electric fields). In our comparisons we consider three versions of Γ: (1) a revised $\Gamma_{\text{eff,cor}}$ expression (Eq. 1) in which the sign error is corrected, (2) a traditional, fixed Γ of 10^{-5} N/m, and (3) the incorrect $\Gamma_{\text{eff,inc}}$ expression (Eq. 3).

In addition to three versions of Γ, we used two values of maximum pore radius, $r_{\text{p,max}}$: 12 nm and 60 nm, which are user-imposed constraints, viz. approximations motivated by the structural complexities of cell membranes compared to lipid vesicle membranes. The $r_{\text{p,max}}$ imposition is partly in recognition of the large fraction of membrane area occupied by membrane proteins, which for a very large pore, would be "swept up" and forced to the rim of the pore, changing at least the effective D_{p} for further pore expansion. Operationally, $r_{\text{p,max}}$ enforces the maximum pore size. A 12 nm maximum is used in the Smith Thesis [1], and leads to consistent results for the conditions used as input to the model, as originally envisioned and presented. Our subsequent use of the 60 nm value is motivated by Krassen et al. 2007 [2], which cites cell membrane structure.

Tables 1 and 2 present cumulative solute transport results obtained with the three versions of Γ (two "effective"; one fixed), and two values of $r_{\text{p,max}}$ for the long and short pulses. Figs. SI-3 - 14 present comparative results in greater detail. These tables and figures show that in most cases, the cumulative solute uptake predictions using different expressions for Γ and $r_{p,max}$ varies within 10 % of the results originally published on July 22, 2014. However, two unanticipated responses were obtained using revised Γ_{eff}. (1) With $r_{\text{p,max}} = 60$ nm a runaway feedback loop occurs during the 1.5 kV/cm, 100 μs pulse (Fig. SI-4): the expansion of pores during a pulse increases Γ_{eff} and significantly decreases W_{surf}, favoring further pore expansion. This results in the rapid expansion of a major subpopulation of pores to $r_{\text{p,max}} = 60$ nm radius, which continue to persist after the pulse instead of decaying with the intended 4 s pore lifetime. However, this runaway pore pileup at $r_{\text{p,max}}$ is not obtained when $\Gamma_{\text{eff,cor}}$ or fixed Γ is used with 12 nm $r_{\text{p,max}}$. (2) Both 12 nm and 60 nm values of $r_{\text{p,max}}$ produce prolonged pore lifetimes after supra-EP by a 40 kV/cm, 10 ns pulse (Figs. SI-10 and 14). The creation of 2.1×10^6 small pores increases the available membrane area, decreasing $A_{l,p}$ and Γ_{eff}. The resulting increase in W_{surf} increases the stability of pores (similar to (1) above) and decreases pore destruction rates. Both of these unanticipated results have not been confirmed by experiment, making it difficult to justify the usage of Γ_{eff}.

For this reason, we have revised the original July 22, 2014 manuscript by providing new results

obtained with the traditional, fixed value of 10^{-5} N/m for Γ, instead of Γ_{eff}. Additionally, we use 12 nm for $r_{\text{p,max}}$ instead of 60 nm, with the understanding that even for large solutes such as cytochrome-c ($r_{\text{s}} \approx 2$ nm), and human or bovine serum albumin ($r_{\text{s}} \approx 4$ nm), the hindrance and partitioning factors differ negligibly for pores of 12 and 60 nm radius. Other measurable quantities such as G_{m}, $U_{\text{m}}(t)$ are dominated by ubiquitous small ions (Na^+, K^+ and Cl^-), which are even less restricted by $r_{\text{p,max}}$.

	N_{cal}	N_{pro}
Fig. SI-3: Original incorrect Γ_{eff} and $r_{\text{p,max}} = 60$ nm	3.3×10^7	3.6×10^7
Fig. SI-4: Revised Γ_{eff} and $r_{\text{p,max}} = 60$ nm	2.5×10^9	2.5×10^9
Fig. SI-5: Fixed Γ and $r_{\text{p,max}} = 60$ nm	3.6×10^7	3.9×10^7
Fig. SI-6: Original incorrect Γ_{eff} and $r_{\text{p,max}} = 12$ nm	3.1×10^7	3.4×10^7
Fig. SI-7: Revised Γ_{eff} and $r_{\text{p,max}} = 12$ nm	3.2×10^7	3.6×10^7
Fig. SI-8: Fixed Γ and $r_{\text{p,max}} = 12$ nm	3.2×10^7	3.5×10^7

Table 1: Key results for the model's response to a 1.5 kV/cm, 100 μs pulse for the three Γ expressions and two $r_{\text{p,max}}$ values.

	N_{cal}	N_{pro}
Fig. SI-9: Original incorrect Γ_{eff} and $r_{\text{p,max}} = 60$ nm	1.3×10^7	7.9×10^8
Fig. SI-10: Revised Γ_{eff} and $r_{\text{p,max}} = 60$ nm	4.9×10^7	1.8×10^9
Fig. SI-11: Fixed Γ and $r_{\text{p,max}} = 60$ nm	2.3×10^7	1.2×10^9
Fig. SI-12: Original incorrect Γ_{eff} and $r_{\text{p,max}} = 12$ nm	1.3×10^7	7.9×10^8
Fig. SI-13: Revised Γ_{eff} and $r_{\text{p,max}} = 12$ nm	4.9×10^7	1.8×10^9
Fig. SI-14: Fixed Γ and $r_{\text{p,max}} = 12$ nm	2.3×10^7	1.2×10^9

Table 2: Table of representative results for models results in response to a 40 kV/cm, 10 ns pulse obtained with different Γ expressions and $r_{\text{p,max}}$ values.

2 Comparative EP and solute transport results for variations in Γ_{eff} and $r_{\text{p,max}}$

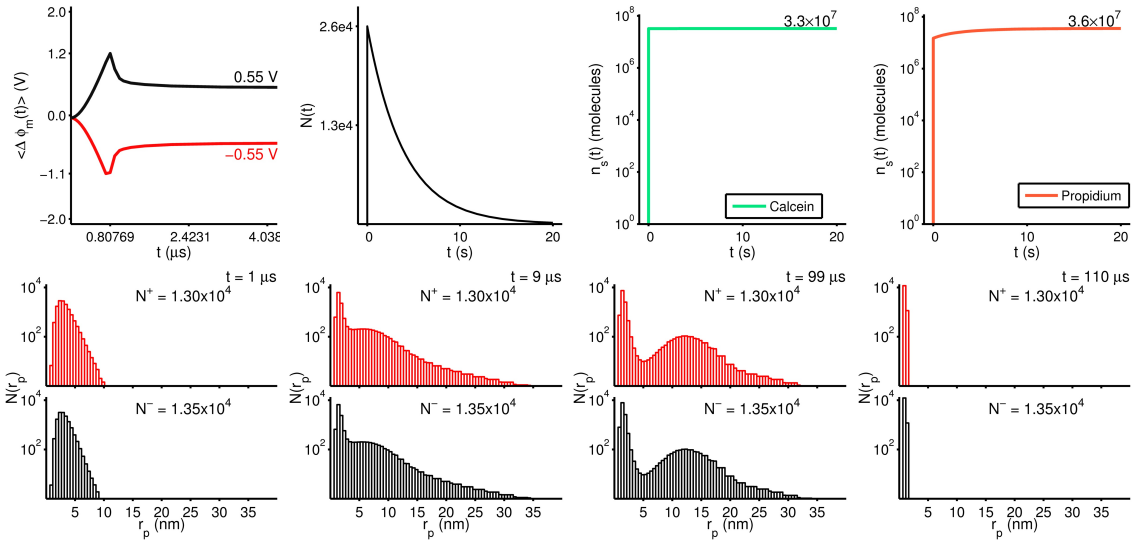

Fig. SI-3 Model response to a 1.5 kV/cm, 100 μs pulse using the $\Gamma_{\text{eff,inc}}$ expression with the sign error and 60 nm $r_{\text{p,max}}$. These results were published in the original July 22, 2014 manuscript.

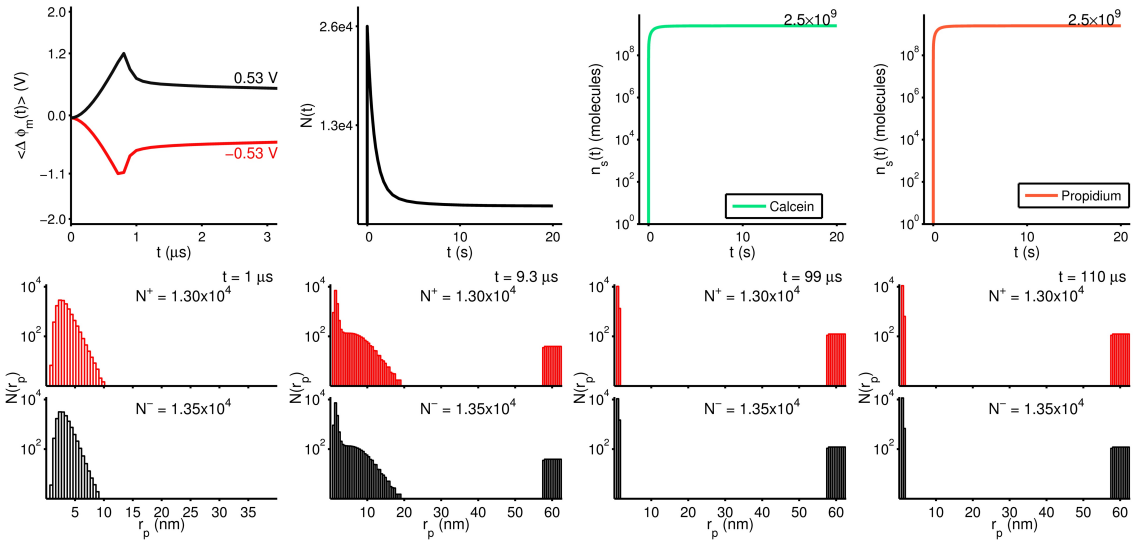

Fig. SI-4 Model response to the long pulse (1.5 kV/cm, 100 μs) using revised Γ_{eff} with 60 nm $r_{\text{p,max}}$. During the pulse, a large subpopulation of pores rapidly expands to 60 nm radius, with some pores reaching $r_{\text{p,max}}$ within 10 μs. This rapid expansion significantly reduces the membrane area available for EP and further reduces the energy for pore expansion. With the resulting runaway feedback loop, all remaining pores expand to $r_{\text{p,max}}$. The resulting change in the pore energy landscape creates a long-lived large pore state, such that the number of pores, $N(t)$ reaches a non-zero asymptote over the 20 s simulation time. The cumulative transport of calcein and propidium reaches intracellular equilibrium amounts of 2.5×10^9 molecules, nearly a 100-fold more than predicted in the original manuscript.

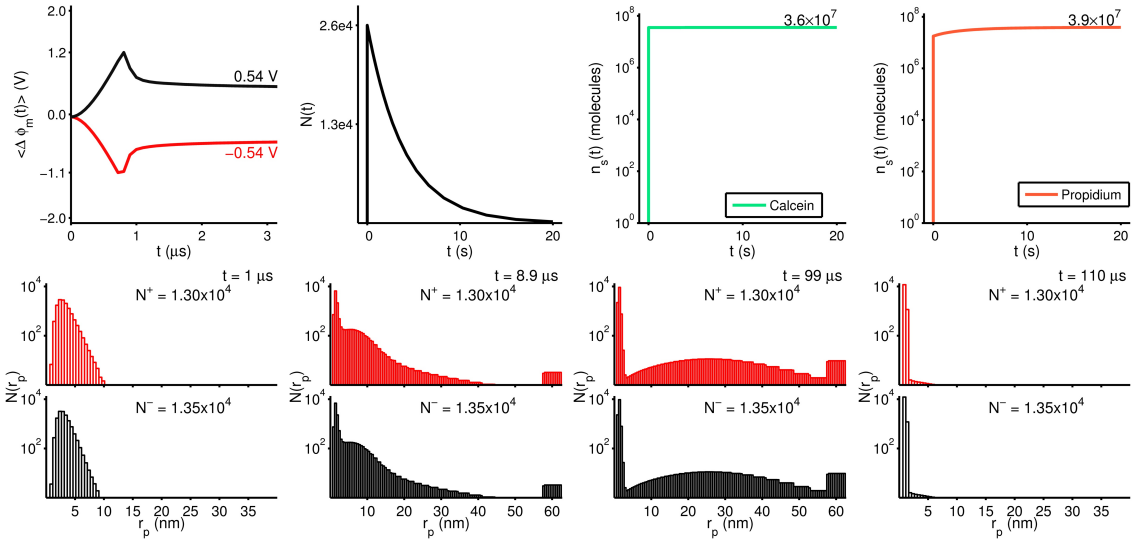

Fig. SI-5 Model response to the long pulse using a traditional, fixed $\Gamma = 10^{-5}$ N/m with 60 nm $r_{\text{p,max}}$. A few pores expand to 60 nm during the pulse, resulting in the transport of 9% more calcein and 8% more propidium than the results published in the original manuscript.

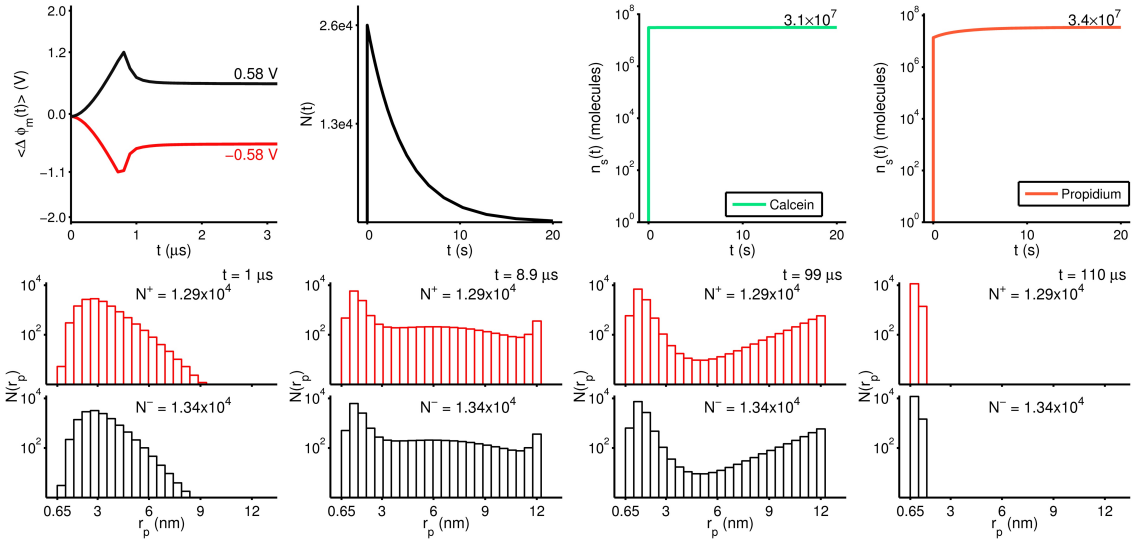

Fig. SI-6 Model response to the long pulse using the original $\Gamma_{\mathrm{eff,inc}}$ expression but with 12 nm $r_{\mathrm{p,max}}$. This smaller value of $r_{\mathrm{p,max}}$ limits the expansion of pores during the pulse, and therefore decreases the amount of drift-dominated solute transport during the pulse. As a result, the cumulative transport of calcein and propidium is 5-6 % less than predicted in the originally published results.

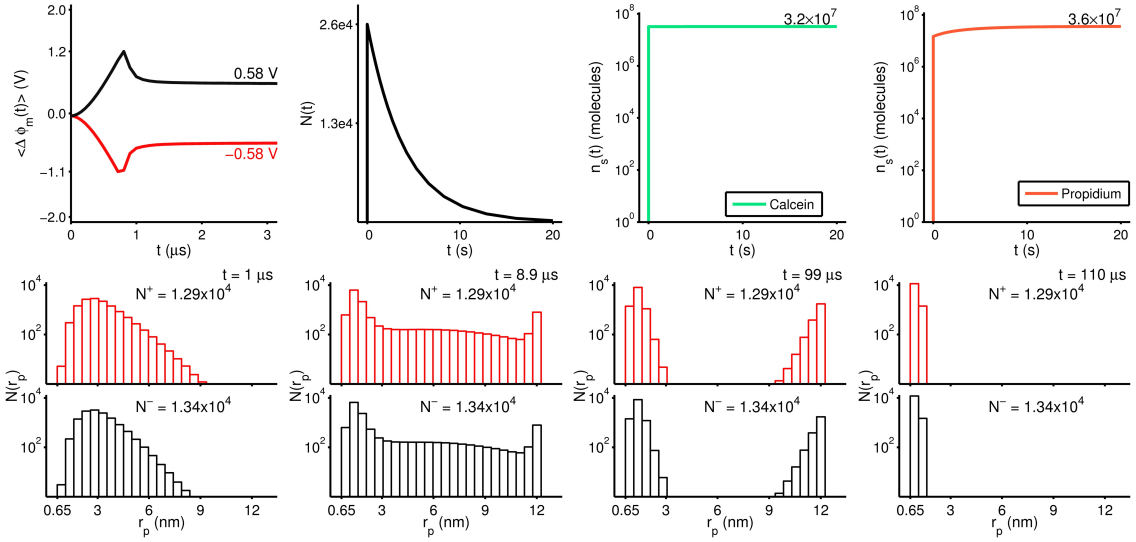

Fig. SI-7 Model response to the long pulse using $\Gamma_{\mathrm{eff,cor}}$ with 12 nm $r_{\mathrm{p,max}}$. Although the use of smaller $r_{\mathrm{p,max}}$ limits pore expansion, the use of revised Γ_{eff} increases the membrane surface tension as pores expand, favoring the expansion of larger pores. These two effects partially counteract, such that the revised Γ_{eff} model with 12 nm $r_{\mathrm{p,max}}$ predicts calcein and propidium uptake within 3% of the originally published values.

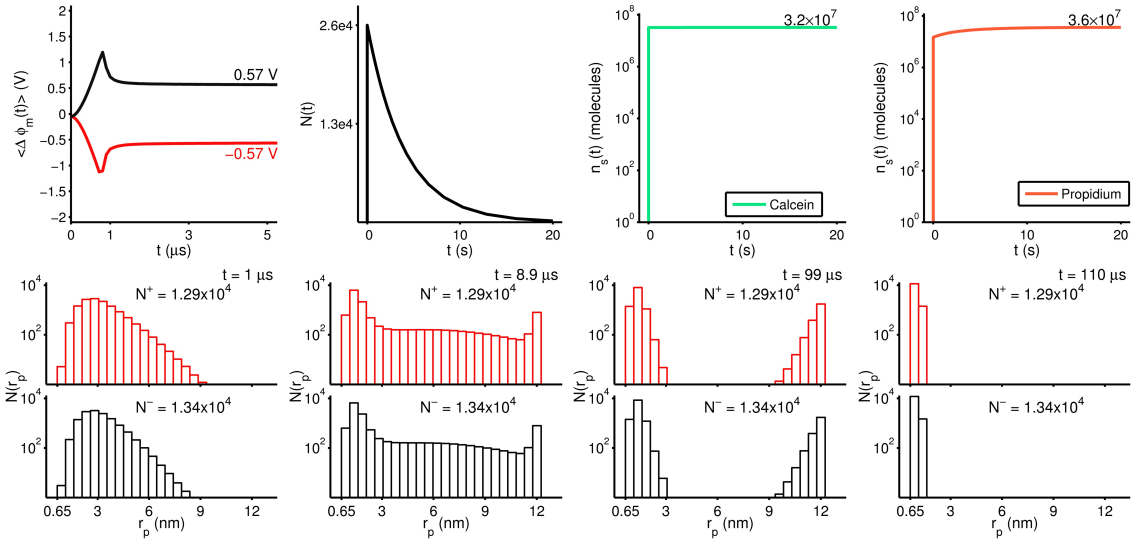

Fig. SI-8 Model response to the long pulse using fixed $\Gamma = 10^{-5}$ N/m with 12 nm $r_{\mathrm{p,max}}$. Fixed Γ favors more pore expansion than $\Gamma_{\mathrm{eff,inc}}$, which partially cancels the decreased pore expansion associated with the smaller $r_{\mathrm{p,max}}$ of 12 nm. This results in cumulative solute uptake within 3% of the originally published results.

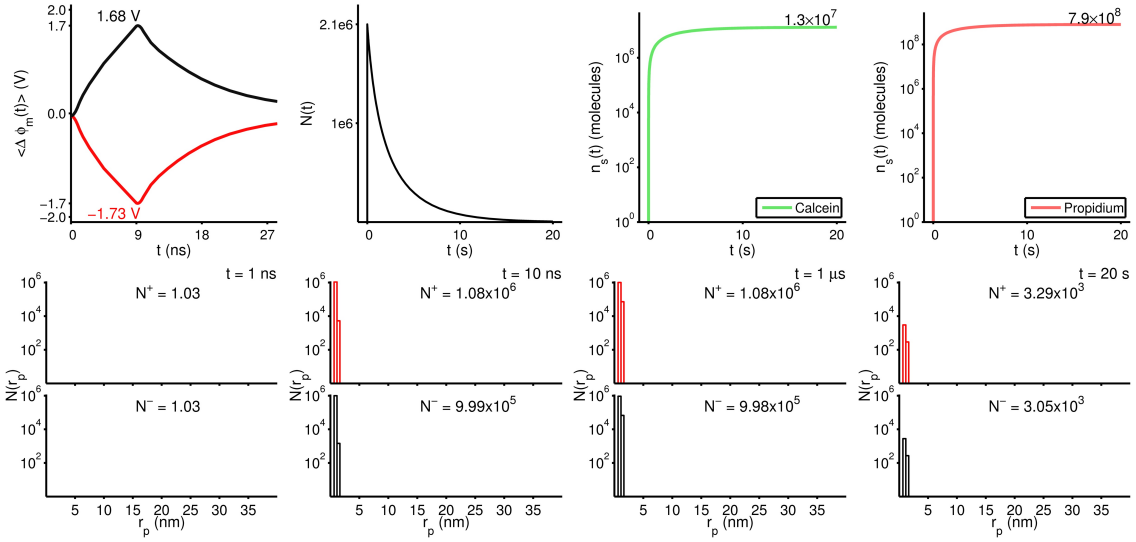

Fig. SI-9 Model response to the short pulse (40 kV/cm, 10 ns) using the incorrect Γ_{eff} expression and 60 nm $r_{\mathrm{p,max}}$, which was published in the original manuscript on July 22, 2014.

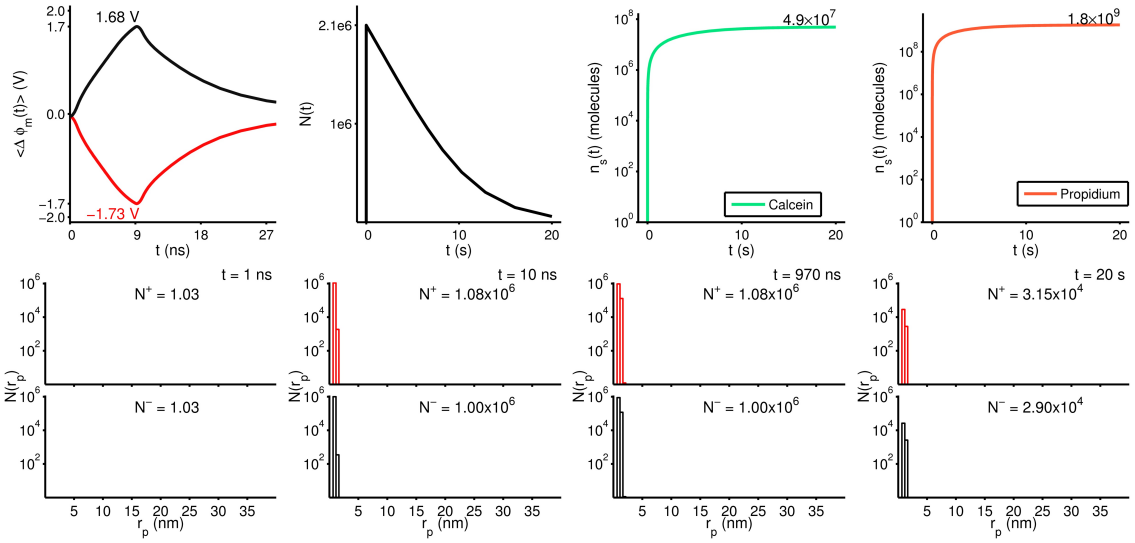

Fig. SI-10 Model response to the short pulse using revised Γ_{eff} and a maximum pore radius of 60 nm $r_{p,max}$. As with the originally published results, the pulse creates 2.1×10^6 small pores. However, with revised Γ_{eff}, these pores yield unintended negative value for the membrane tension, such that the resulting change in pore energy increases the barrier to pore destruction and increases the pore lifetime. As a result, the total pore number $N(t)$, decays with a pore lifetime, τ_p longer than 4 s. The pore size histograms show more than 4 times as many pores remain at $t = 20$ s for revised Γ_{eff} than for the original incorrect Γ_{eff} expression. As a consequence, the revised Γ_{eff} model predicts 380% more calcein uptake and 230% more propidium uptake than the originally published results (SI Fig. 9).

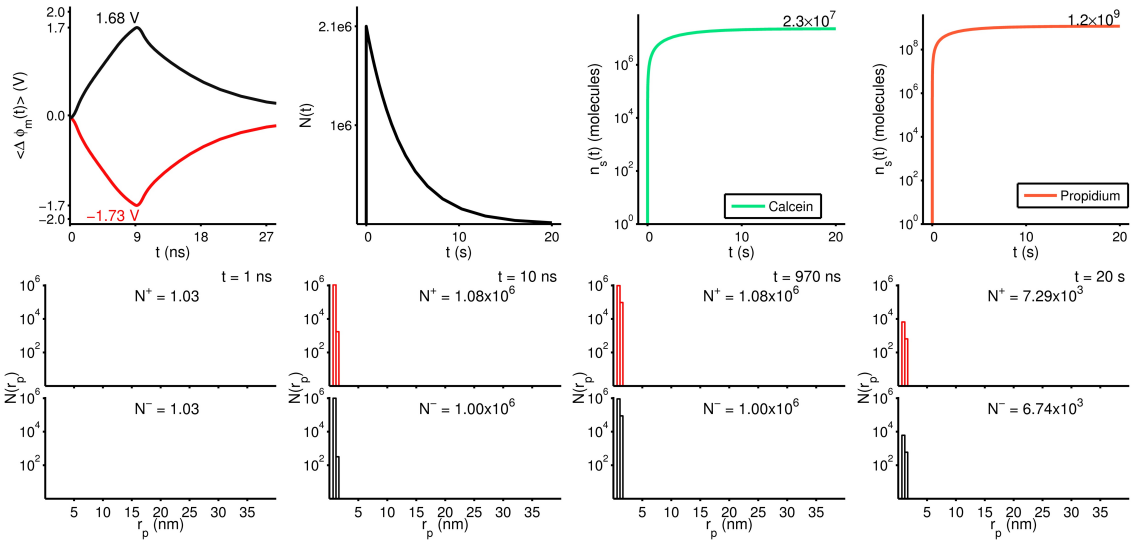

Fig. SI-11 Model response to a 40 kV/cm, 10 ns pulse using fixed $\Gamma = 10^{-5}$ N/m with 60 nm $r_{\text{p,max}}$. The decay rate for $N(t)$ is faster than that of the corrected Γ_{eff} case, but the pore lifetime is still longer than the 4 s pore lifetime presented in the original manuscript. The resulting solute transport results show cumulative calcein uptake increases by 76%, and propidium cumulative uptake increases by 52% compared to the originally published results.

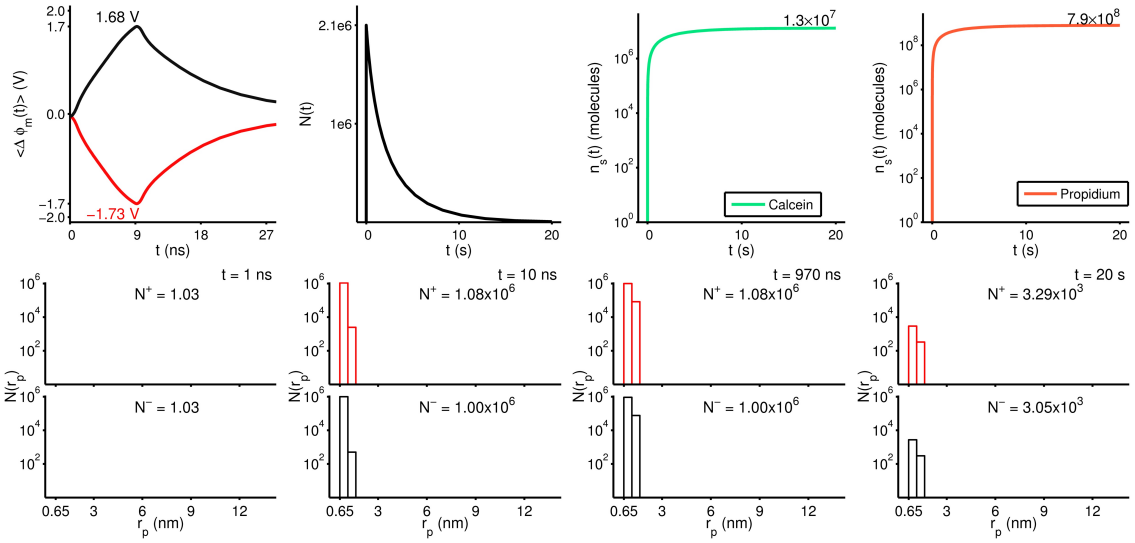

Fig. SI-12 Model response to the short pulse using the incorrect Γ_{eff} expression and 12 nm $r_{\text{p,max}}$. Unlike the long pulse response, pore expansion beyond 3 nm is not observed. For this reason the 12 nm $r_{\text{p,max}}$ constraint yields results indistinguishable from those obtained with 60 nm maximum radius in the originally published manuscript.

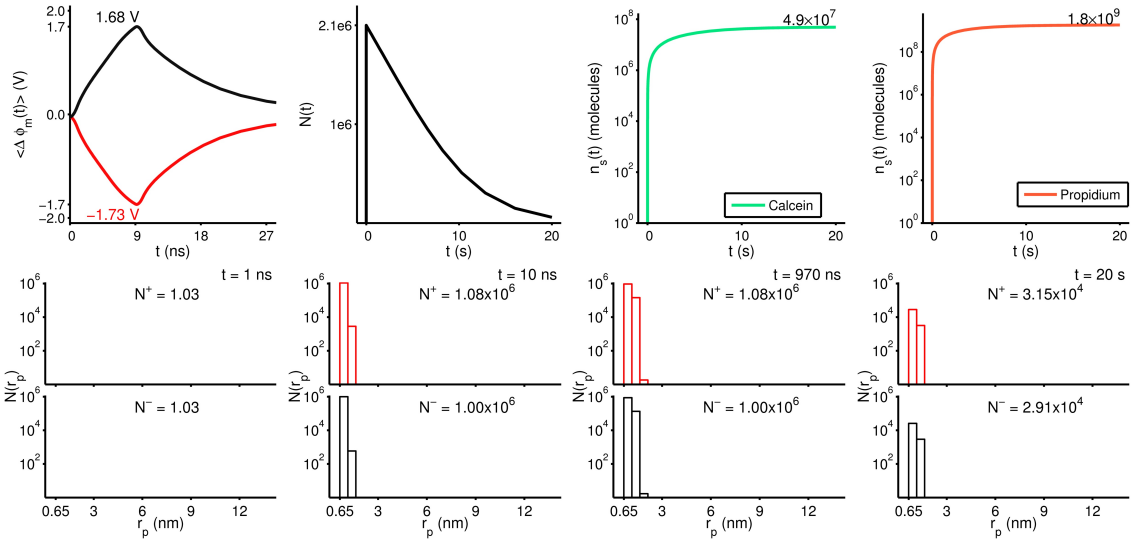

Fig. SI-13 Model response to the short pulse using the revised tension expression, $\Gamma_{\text{eff,cor}}$, with 12 nm $r_{\text{p,max}}$. The cumulative solute uptake results and increased pore lifetime behavior are identical to those obtained with the revised Γ_{eff} version and 60 nm $r_{p,max}$ (SI Fig. 10). The rate of pore destruction is much slower than that of a 4 s pore lifetime (SI Fig. 9), and as a result, 380% more calcein uptake and 230% more propidium uptake is predicted than in the originally published results.

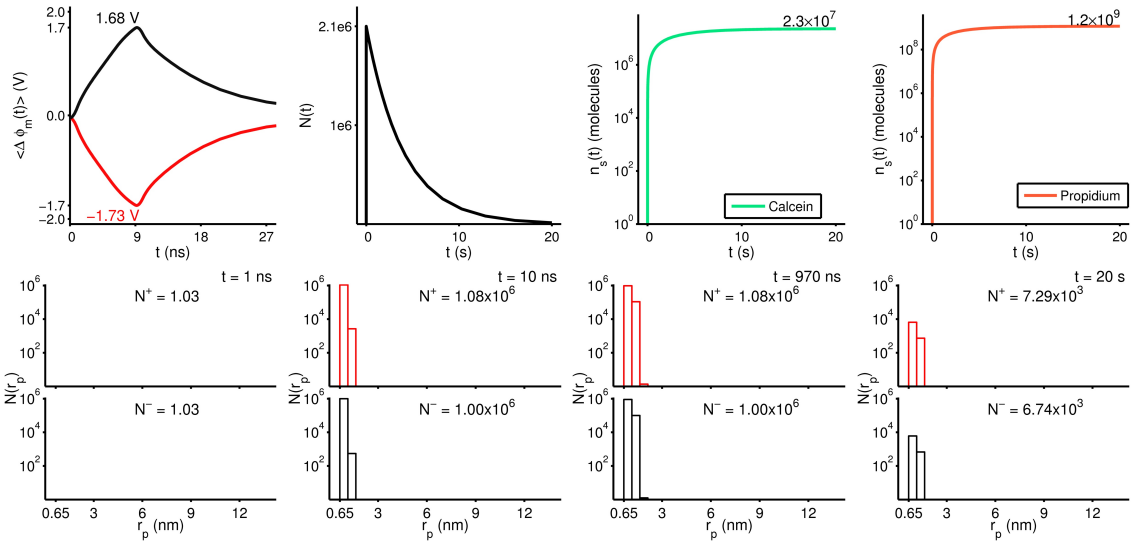

Fig. SI-14 Model response to the short pulse using fixed $\Gamma_{\text{eff}} = 10^{-5}$ N/m with 12 nm $r_{\text{p,max}}$. These results are identical to the revised Γ_{eff} case and 60 nm $r_{\text{p,max}}$ (SI Fig. 11). The rate of pore destruction is slower than that for a 4 s pore lifetime (SI Fig. 12), resulting in a 76% increase in calcein uptake and a 52% increase in propidium compared to the originally published results.

3 Comparative solute transport results for pulses used in Canatella 2001 and Puc 2003

Table 3 and Figs. SI-15-22 present comparative uptake of 10 μM extracellular calcein for exponential pulses ranging from 50 μs to 21 ms [6]. Additionally, Table 4 and Figs. SI-23-26 present comparative uptake of 1 mM extracellular Lucifer Yellow for 100 μs and 1 ms trapezoidal pulses, based on [7]. These two sets of experiments are the basis of the original parametric optimization of the model [1]. As with Tables 1-2 and Figs. SI 3-14, we compare the resulting solute transport predictions obtained with $\Gamma_{\text{eff,inc}}$ (Eq. 3; incorrect expression for Γ_{eff}), fixed Γ, and revised $\Gamma_{\text{eff,cor}}$. For these comparisons, we use only 12 nm $r_{\text{p,max}}$, as established in the previous section.

For eight pulses ranging from 50 μs to 21 ms used in [6] and the 100 μs and 1 ms trapezoidal pulses used in [7], the resulting solute uptake predictions for fixed Γ and revised Γ_{eff} are within 20% of the solute uptake predictions made with incorrect Γ_{eff}. The model parameters are as described in Table 7.1 of [1] (i.e. $r_{cell} = 11$ μm, $\sigma_e = 1.29$ S/m for Canatella et al. 2001), with the exception that integral charge number of -4 was used for calcein instead of -3.61 (an ensemble average [1]). Similarly, for the two Puc et al. 2003 pulses, $r_{cell} = 8.55$ μm and $\sigma_e = 1.58$ S/m.

	$\Gamma_{\text{eff,inc}}$ N_{cal}	fixed Γ N_{cal}	$\Gamma_{\text{eff,cor}}$ N_{cal}
Fig. SI-15: 3.3 kV/cm, 50 μs pulse	1.2×10^5	1.3×10^5	1.4×10^5
Fig. SI-16: 3.1 kV/cm, 90 μs pulse	1.8×10^5	1.9×10^5	2.1×10^5
Fig. SI-17: 1.2 kV/cm, 500 μs pulse	6.1×10^5	6.0×10^5	6.0×10^5
Fig. SI-18: 1.8 kV/cm, 1.1 ms pulse	2.4×10^6	2.3×10^6	2.4×10^6
Fig. SI-19: 1.3 kV/cm, 2.8 ms pulse	5.0×10^6	4.9×10^6	5.0×10^6
Fig. SI-20: 1.2 kV/cm, 5.3 ms pulse	9.1×10^6	9.1×10^6	9.2×10^6
Fig. SI-21: 1.0 kV/cm, 10 ms pulse	1.4×10^7	1.4×10^7	1.4×10^7
Fig. SI-22: 0.9 kV/cm, 21 ms pulse	2.3×10^7	2.3×10^7	2.3×10^7

Table 3: Table of calcein uptake results for the model response to Canatella et al. 2001 [6] pulses using three different expressions for the membrane surface tension, Γ.

	$\Gamma_{\text{eff,inc}}$ N_{LY}	fixed Γ N_{LY}	$\Gamma_{\text{eff,cor}}$ N_{LY}
Fig. SI-23: 1.0 kV/cm, 100 μs pulse	1.4×10^7	1.4×10^7	1.5×10^7
Fig. SI-24: 1.0 kV/cm, 1 ms pulse	6.9×10^7	7.0×10^7	7.1×10^7
Fig. SI-25: 2.0 kV/cm, 100 μs pulse	5.2×10^7	5.3×10^7	5.4×10^7
Fig. SI-26: 2.0 kV/cm, 1 ms pulse	2.0×10^8	2.0×10^8	2.0×10^8

Table 4: Table of Lucifer Yellow uptake results for the model responses to Puc et al. 2003 [7] pulses using different Γ expressions.

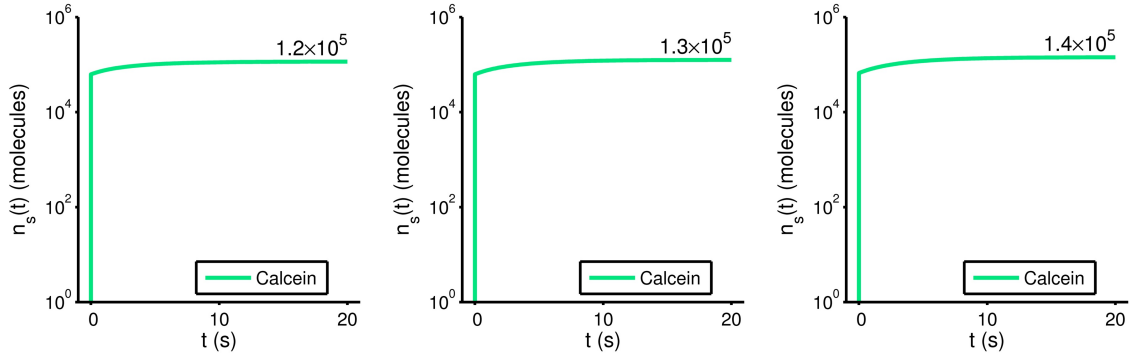

Fig. SI-15 3.3 kV/cm, 50 μs exponential pulse: Predicted calcein uptake using the incorrect Γ_{eff} (left), fixed $\Gamma = 10^{-5}$ N/m (center), and revised Γ_{eff} (right). Each of these results were obtained with $r_{\text{p,max}} = 12$ nm.

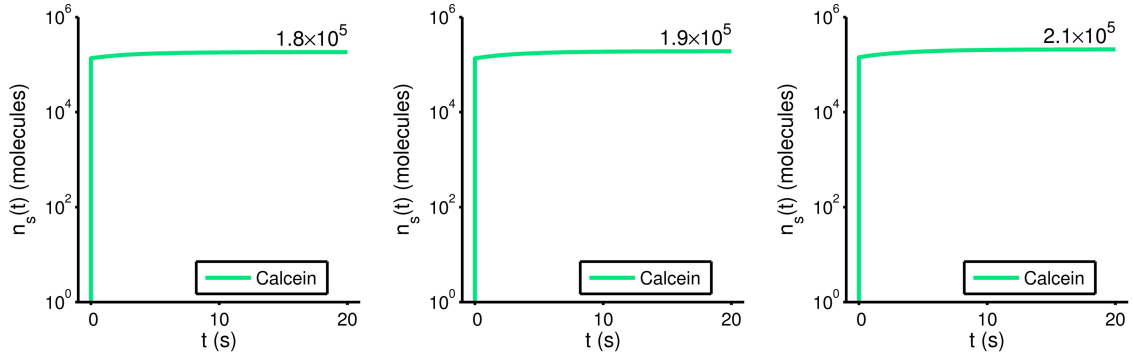

Fig. SI-16 3.1 kV/cm, 90 μs exponential pulse: Predicted calcein uptake using the incorrect Γ_{eff} (left), fixed $\Gamma = 10^{-5}$ N/m (center), and revised Γ_{eff} (right). Each of these results were obtained with $r_{\text{p,max}} = 12$ nm.

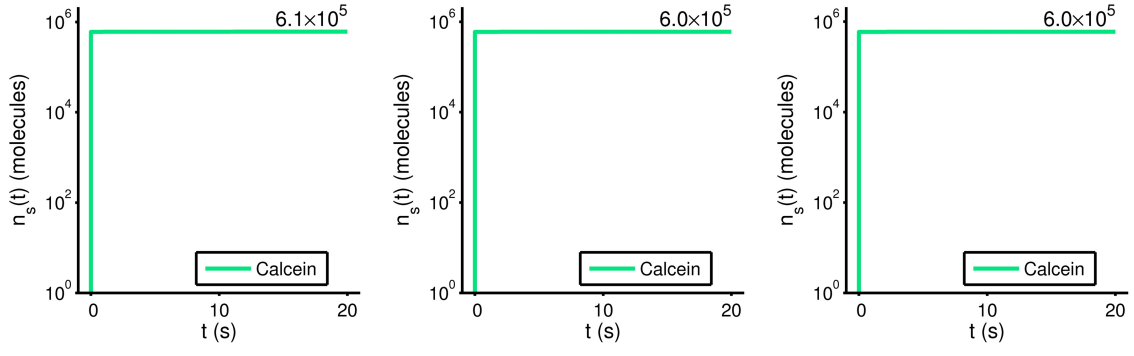

Fig. SI-17 1.2 kV/cm, 500 μs exponential pulse: Predicted calcein uptake using the incorrect Γ_{eff} (left), fixed $\Gamma = 10^{-5}$ N/m (center), and revised Γ_{eff} (right). Each of these results were obtained with $r_{\text{p,max}} = 12$ nm.

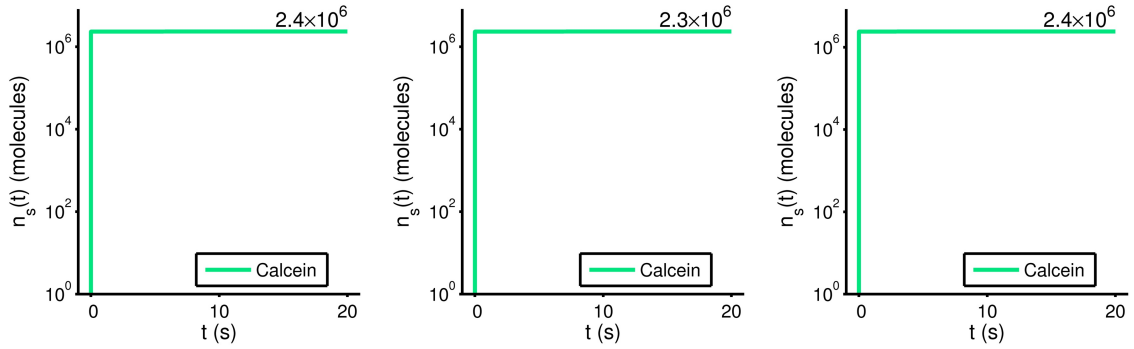

Fig. SI-18 1.8 kV/cm, 1.1 ms exponential pulse: Predicted calcein uptake using the incorrect Γ_{eff} (left), fixed $\Gamma = 10^{-5}$ N/m (center), and revised Γ_{eff}. Each of these results were obtained with $r_{\text{p,max}} = 12$ nm.

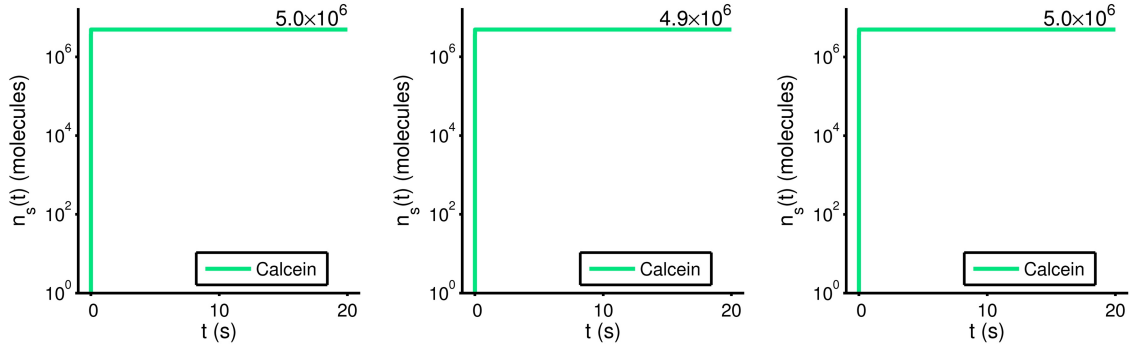

Fig. SI-19 1.3 kV/cm, 2.8 ms exponential pulse: Predicted calcein uptake using the incorrect Γ_{eff} (left), fixed $\Gamma = 10^{-5}$ N/m (center), and revised Γ_{eff} (right). Each of these results were obtained with $r_{\text{p,max}} = 12$ nm.

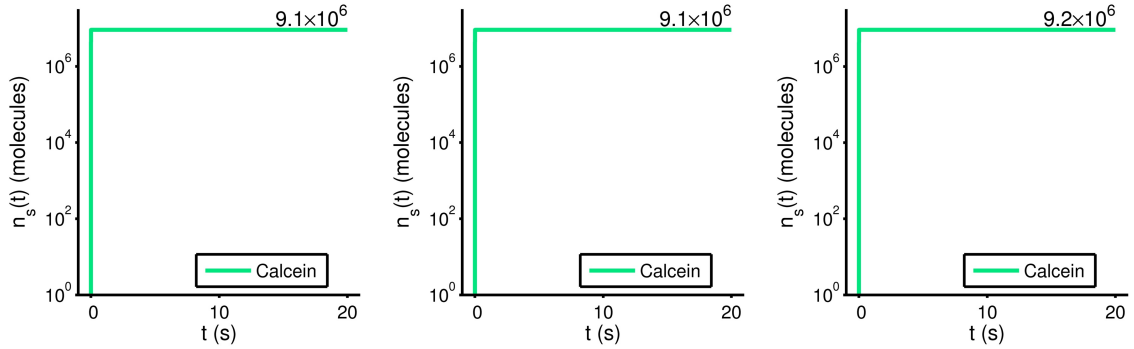

Fig. SI-20 1.2 kV/cm, 5.3 ms exponential pulse: Predicted calcein uptake using the incorrect Γ_{eff} (left), fixed $\Gamma = 10^{-5}$ N/m (center), and revised Γ_{eff} (right). Each of these results were obtained with $r_{\text{p,max}} = 12$ nm.

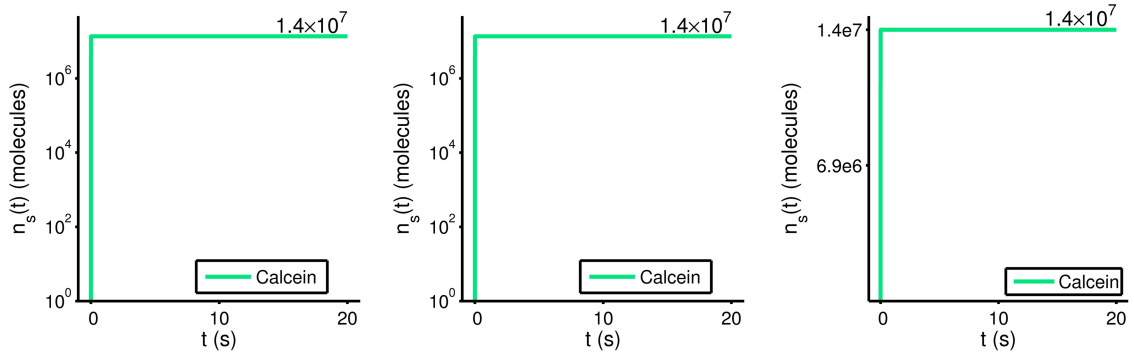

Fig. SI-21 1.0 kV/cm, 10 ms exponential pulse: Predicted calcein uptake using the incorrect Γ_{eff} (left), fixed $\Gamma = 10^{-5}$ N/m (center), and revised Γ_{eff} (right). Each of these results were obtained with $r_{\text{p,max}} = 12$ nm.

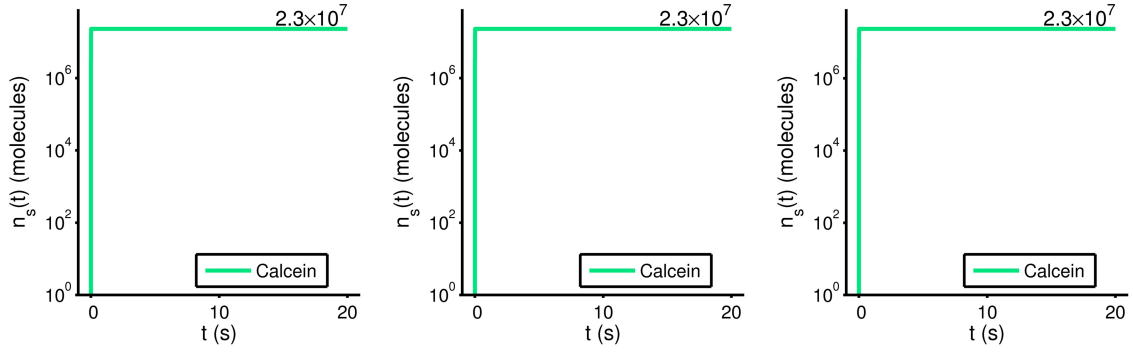

Fig. SI-22 0.9 kV/cm, 21 ms exponential pulse: Predicted calcein uptake using the incorrect Γ_{eff} (left), fixed $\Gamma = 10^{-5}$ N/m (center), and revised Γ_{eff} (right). Each of these results were obtained with $r_{\text{p,max}} = 12$ nm.

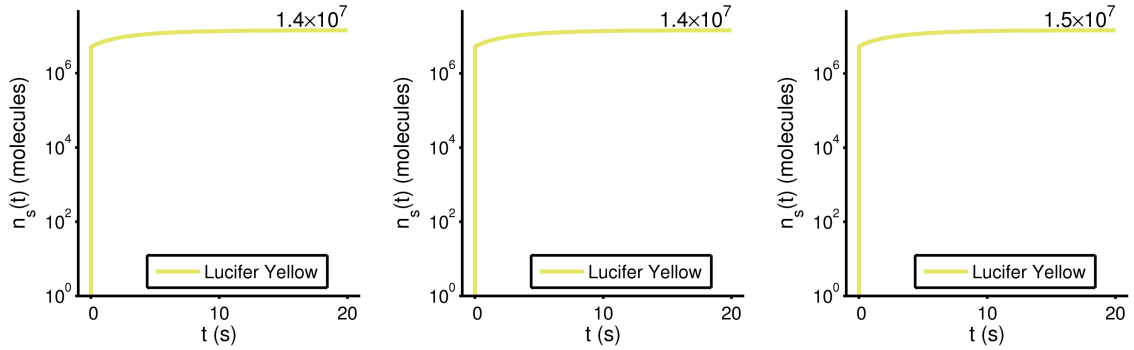

Fig. SI-23 1.0 kV/cm, 100 μs trapezoidal pulse: Predicted Lucifer Yellow uptake using the incorrect Γ_{eff} (left), fixed $\Gamma = 10^{-5}$ N/m (center), and revised Γ_{eff} (right). Each of these results were obtained with $r_{\text{p,max}} = 12$ nm.

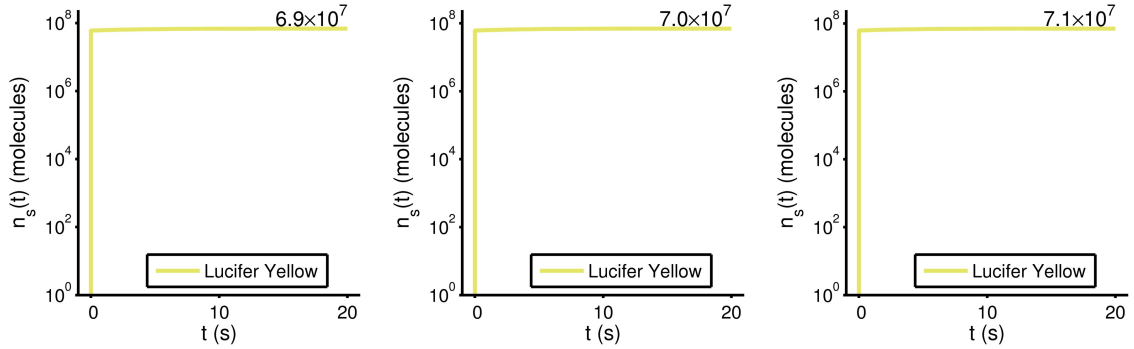

Fig. SI-24 1.0 kV/cm, 1 ms trapezoidal pulse: Predicted Lucifer Yellow uptake using the incorrect Γ_{eff} (left), fixed $\Gamma = 10^{-5}$ N/m (center), and revised Γ_{eff} (right). Each of these results were obtained with $r_{\text{p,max}} = 12$ nm.

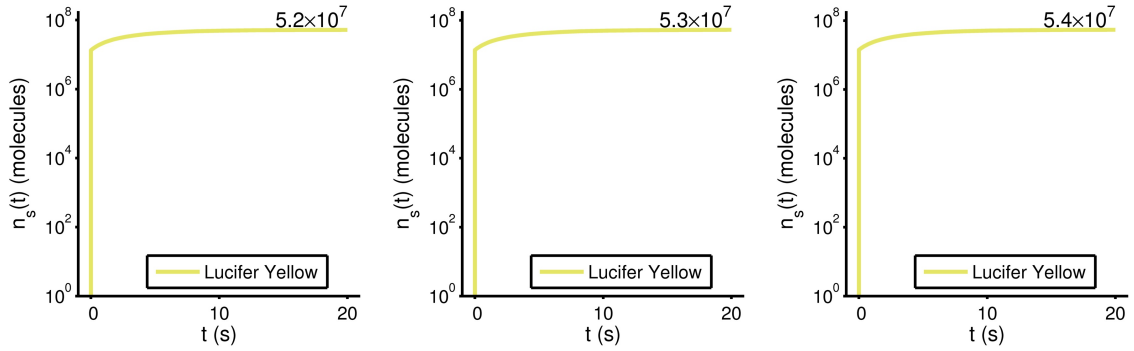

Fig. SI-25 2.0 kV/cm, 100 μs trapezoidal pulse: Predicted Lucifer Yellow uptake using the incorrect Γ_{eff} (left), fixed $\Gamma = 10^{-5}$ N/m (center), and revised Γ_{eff} (right). Each of these results were obtained with $r_{\text{p,max}} = 12$ nm.

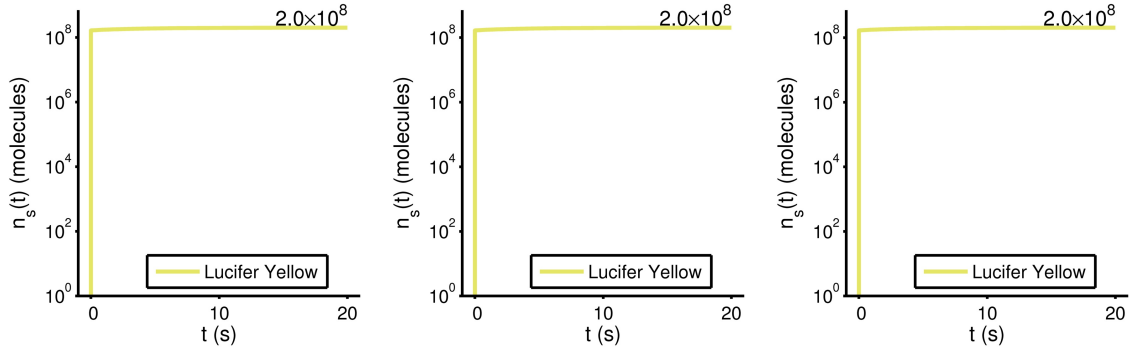

Fig. SI-26 2.0 kV/cm, 1 ms trapezoidal pulse: Predicted Lucifer Yellow uptake using the incorrect Γ_{eff} (left), fixed $\Gamma = 10^{-5}$ N/m (center), and revised Γ_{eff} (right). Each of these results were obtained with $r_{\text{p,max}} = 12$ nm.

4 Summary

Since the original publication of our manuscript in JMB on July 22, 2014, an error has been found in the implementation of effective membrane surface tension, Γ_{eff}, in the model. To address this error, additional model results have been obtained with both a revised expression for Γ_{eff} (as it was originally intended) and a traditional fixed value of Γ. We have taken the additional step of obtaining comparative results for a maximum pore radius, $r_{\text{p,max}}$ of 12 nm, in addition to the 60 nm $r_{\text{p,max}}$ value used in the original manuscript. Results are presented for six combinations of three Γ expressions and two $r_{\text{p,max}}$ values, for the 1.5 kV/cm, 100 μs and 40 kV/cm, 10 ns pulses presented in the manuscript. Tables 1-2 compile the cumulative transport results for calcein and propidium for comparison, and Figs. SI-3-14 provide greater detail of the model's behavior.

For most cases, differences in EP behavior and solute transport are insignificant. However, for a few outstanding cases, usage of revised Γ_{eff} yields significant changes in EP response (runaway pore expansion, elongated pore lifetime). Due to these unintended effects from revised Γ_{eff}, we have chosen to revise the original manuscript with results obtained with fixed $\Gamma = 10^{-5}$ N/m and 12 nm r_{max}. For completeness, we also model the pulse and cell conditions [6, 7] originally used to test and calibrate the present model [1], and present these results in Tables 3-4 and Figs. SI-15-26. For these results, the same three variations of Γ were used, but with only 12 nm $r_{\text{p,max}}$.

Based on these comparative results, we have decided to use traditional, fixed Γ with 12 nm $r_{\text{p,max}}$ for the publication, instead of revised Γ_{eff} with 60 nm $r_{\text{p,max}}$. Our choice of fixed Γ with 12 nm $r_{\text{p,max}}$ yields some differences in pore size distributions, but these differences are not experimentally measurable, and do not change the fundamental conclusions of the original manuscript.

References

[1] K. C. Smith, *A unified model of electroporation and molecular transport.* Massachusetts Institute of Technology, http://dspace.mit.edu/bitstream/handle/1721.1/63085/725958797.pdf.

[2] H. Krassen, U. Pliquett, and E. Neumann, "Nonlinear current - voltage relationship of the plasma membrane of single CHO cells," *Bioelectrochemistry*, vol. 70, pp. 71–77, 2007.

[3] R. S. Son, K. C. Smith, T. R. Gowrishankar, and J. C. Weaver, "Gaining access to intracellular compartments by electroporation," *Proc. EBTT, Ljubljana, Slovenia, Nov 17 - 23, 2013*, pp. 99–107.

[4] K. C. Smith, R. S. Son, T. R. Gowrishankar, and J. C. Weaver, "Emergence of a large pore subpopulation during electroporating pulses," *Bioelectrochemistry*, vol. 100, pp. 3 – 10, 2014.

[5] R. S. Son, K. C. Smith, T. R. Gowrishankar, P. T. Vernier, and J. C. Weaver, "Basic features of a cell electroporation model: Illustrative behavior for two very different pulses," *J. Membrane Biol.*, 2014.

[6] P. J. Canatella, J. F. Karr, J. A. Petros, and M. R. Prausnitz, "Quantitative study of electroporation-mediated molecular uptake and cell viability," *Biophysical J.*, vol. 80, pp. 755–764, 2001.

[7] M. Puc, J. Kotnik, L. M. Mir, and D. Miklavčič, "Quantitative model of small molecules uptake after in vitro cell electropermeabilization," *Bioelectrochemistry*, vol. 60, pp. 1–10, 2003.

[8] J. C. Neu, K. C. Smith, and W. Krassowska, "Electrical energy required to form large conducting pores," *Bioelectrochemistry*, vol. 60, pp. 107–114, 2003.

[9] T. R. Gowrishankar, A. T. Esser, Z. Vasilkoski, K. C. Smith, and J. C. Weaver, "Microdosimetry for conventional and supra-electroporation in cells with organelles," *Biochem. Biophys. Res. Commun.*, vol. 341, pp. 1266–1276, 2006.

[10] S. Talele, P. Gaynor, M. J. Cree, and J. van Ekeran, "Modelling single cell electroporation with bipolar pulse parameters and dynamic pore radii," *J. Electrostatics*, vol. 68, pp. 261–274, 2010.

[11] A. T. Esser, K. C. Smith, T. R. Gowrishankar, Z. Vasilkoski, and J. C. Weaver, "Mechanisms for the intracellular manipulation of organelles by conventional electroporation," *Biophys. J.*, vol. 98, pp. 2506–2514, 2010.